

# WILEY

## Online Proofing System

### Enabling the Adobe PDF Viewer

In order to proof your article Adobe Reader or Adobe Acrobat needs to be your browser's default PDF viewer. See how to set this up for Internet Explorer, Firefox, and Safari at <https://helpx.adobe.com/acrobat/using/display-pdf-in-browser.html>

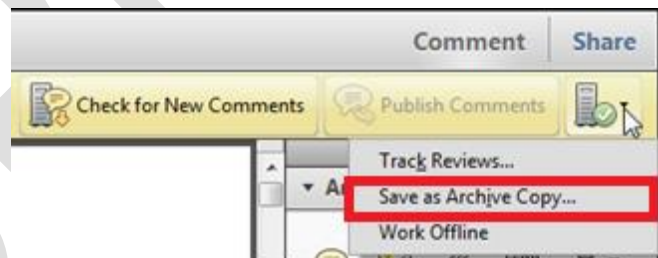
Google Chrome and Microsoft Edge do not support Adobe Reader or Adobe Acrobat as a PDF Viewer. We recommend using Internet Explorer, Firefox, or Safari.

**1.** Mark your corrections, changes, and query responses using the Annotation Tools outlined on the next 2 pages.

**2.** Save your proof corrections by clicking the “Publish Comments” button in the yellow banner above. Corrections don’t have to be marked in one sitting. You can publish comments and log back in at a later time to add and publish more comments before you click the “Complete Proof Review” button.



**3.** When your proof review is complete we recommend you download a copy of your annotated proof for reference in any future correspondence concerning the article before publication. You can do this by clicking on the icon to the right of the ‘Publish Comments’ button and selecting ‘Save as Archive Copy...’.



**IMPORTANT:** Did you reply to all author queries found on the last page of your proof?

**IMPORTANT:** Did you click the “Publish Comments” button to save all your corrections? Any unpublished comments will be lost.

**IMPORTANT:** Once you click “Complete Proof Review” you will not be able to add or publish additional corrections.

**4.** When your proof review is complete and all corrections have been published to the server by clicking the “Publish Comments” button, please click the “Complete Proof Review” button appearing above the proof in your web browser window.

COMPLETE PROOF REVIEW

## Author Query Form

**Journal: International Journal of Energy Research**

**Article: er\_3847**

Dear Author,

During the copyediting of your paper, the following queries arose. Please respond to these by annotating your proofs with the necessary changes/additions.

- If you intend to annotate your proof electronically, please refer to the E-annotation guidelines.
- If you intend to annotate your proof by means of hard-copy mark-up, please use the standard proofing marks. If manually writing corrections on your proof and returning it by fax, do not write too close to the edge of the paper. Please remember that illegible mark-ups may delay publication.

Whether you opt for hard-copy or electronic annotation of your proofs, we recommend that you provide additional clarification of answers to queries by entering your answers on the query sheet, in addition to the text mark-up.

| Query No. | Query   | Remark  |
|-----------|---|---|
| Q1        | AUTHOR: Please confirm that given names (red) and surnames/family names (green) have been identified correctly. | confirmed   |
| Q2        | AUTHOR: Please verify that the linked ORCID identifiers are correct for each author.                            | confirmed   |
| Q3        | AUTHOR: Please provide keywords.  | lithium-ion battery,<br>MHPA,<br>thermal management |

RESEARCH ARTICLE

# Thermal management system of lithium-ion battery module based on micro heat pipe array

Xin Ye  | Yaohua Zhao | Zhenhua Quan

Department of Building Environment and Facility Engineering, College of Architecture and Civil Engineering, Beijing University of Technology, No. 100 Pingleyuan, Chaoyang District, Beijing 100124, China

## Correspondence

Xin Ye, Department of Building Environment and Facility Engineering, College of Architecture and Civil Engineering, Beijing University of Technology, No. 100 Pingleyuan, Chaoyang District, Beijing 100124, China.  
Email: stellaye@126.com

## Summary

Temperature affects the performance of electric vehicle battery. To solve this problem, micro heat pipe arrays are utilized in a thermal management system that cools and heats battery modules. In the present study, the heat generation of a battery module during a charge-discharge cycle under a constant current of 36 A (2C) was computed. Then, the cooling area of the condenser was calculated and experimentally validated. At rates of 1C and 2C, the thermal management system effectively reduced the temperature of the module to less than 40°C, and the temperature difference was controlled less than 5°C between battery surfaces of the module. A heating plate with 30-W power effectively improved charge performance at low temperature within a short heating time and with uniform temperature distribution. Charge capacity obviously increased after heating when battery temperature was below 0°C. This study presents a new way to enhance the stability [Colour figure can be viewed at [wileyonlinelibrary.com](http://wileyonlinelibrary.com)] and safety of a battery module during the continuous charge-discharge cycle at high temperatures and low temperatures accordingly.

## 1 | INTRODUCTION

The technology of electric vehicles (EVs), has been rapidly developed in recent years.<sup>1</sup> The security issues of batteries restrict the further development of EVs.<sup>2</sup> The charge and discharge process of a lithium-ion battery is a complex internal chemical reaction that generates heat.<sup>3,4</sup> The rapid accumulation of heat will inevitably increase the internal temperature of the battery. Elevated temperatures accelerate corrosion, thus decreasing battery life.<sup>5</sup> Operating batteries at low temperature, however, reduces power output in that electrochemical reactions are suppressed. The temperature within a battery cell must be kept uniform because variations in temperature will cause electrochemical reactions to be proceeded at different rates in different regions of the cell and subsequently lead to incomplete energy utilization.<sup>6</sup> Excessively high, low, or uneven temperature will do harm to battery performance, and therefore, a reasonable battery thermal management

system with which it cools down under high-temperature conditions, heats up under low-temperature conditions, and has local thermal control must be designed.

Thanh-Ha et al<sup>7</sup> reported that natural or forced convection with air could not effectively solve the problem of temperature increase. Ji et al<sup>8</sup> noted that heat transfers slowly from air to battery and caused the uneven distribution of temperature in the battery. Although air TMS appears simple, it is actually complicated. Nelson et al<sup>9</sup> compared the TMS effects of silicone electrolyte fluid with air to verify that the liquid medium is superior to air in heating and cooling. TMS that utilizes fluid, however, is relatively complex, heavyweight, potentially leaky, and difficult to maintain. Khateeb et al<sup>10</sup> used phase change material (PCM) (melting point 40°C–44°C) as the TMS of Li-ion battery packs. Nevertheless, the quality was up to 28.6% of the battery, and heat accumulated due to the low thermal conductivity of the PCM.<sup>11</sup> Swanepoel<sup>12</sup> designed a pulsating heat pipe as the TMS of an Optima

Spirecell (12 V, 65 Ah) lead acid battery, which had strict requirements for the diameter of heat pipe. Even the diameter of the heat pipe meets the requirements, there is only line contact between the surface of this conventional circular heat pipe and battery which causes low heat transfer efficiency.

Each heat pipe in a micro heat pipe array (MHPA) runs independently with good thermal stability and strong heat transport capability.<sup>13</sup> TMS based on MHPA is simple, flexible, lightweight, and does not require extra fan power. Moreover, TMS exhibits high thermal conductivity and large contact area, which is suitable for a battery module in a compact and limited space that requires cooling and heating. In this study, TMS for a Li-ion battery module was designed based on a 3-mm-thick MHPA.

## 2 | TMS

### 2.1 | Battery module

In this study, 16 cells (18 Ah, rectangular, 165 mm × 70 mm × 27 mm) in a series were used as temperature test samples for the charge-discharge process. The battery was covered with electrical insulation. The space between each cell was 3 mm. A one-fourth battery module, which comprised 4 cells that were used for temperature tests, approximately represented the entire module in boundary condition symmetry. The battery setup is illustrated in Figure 1A. Figure 1B shows 1 side of the thermocouple. Cells 1 and 2 were set on both sides of the thermocouple for a total 18 points. Nine points were arranged evenly on the 1 side of cells 3 and 4.

### 2.2 | MHPA

The experimental study<sup>14</sup> proved that MHPA exhibits isothermal characteristic and fast thermal response. Figure 2 presents the internal structure of MHPA. There are many



FIGURE 2 Photograph of MHPAs

inner micro-grooves (or micro-fins) in each micro heat pipe to enhance the heat transfer. In this setup, even if 1 pipe is damaged, the other independent pipes continue working properly.

Wang et al<sup>15</sup> applied MHPA in battery cooling system but only carried on the simulation analysis. Wang et al<sup>16</sup> applied MHPA to a single LED heat dissipation and verified the effective heat capacity of the plant. This paper applied MHPA to module cooling experiment of multiple heat sources.

### 2.3 | TMS design

#### 2.3.1 | Cooling method

The evaporation section of the MHPA fitted closely to the cell surface and was filled with thermal silicone. The condensation section was exposed to air. The heat generated by the battery during the charge-discharge process was transmitted through the MHPA internal channel and then transferred to air through convection. As shown in Figure 3.

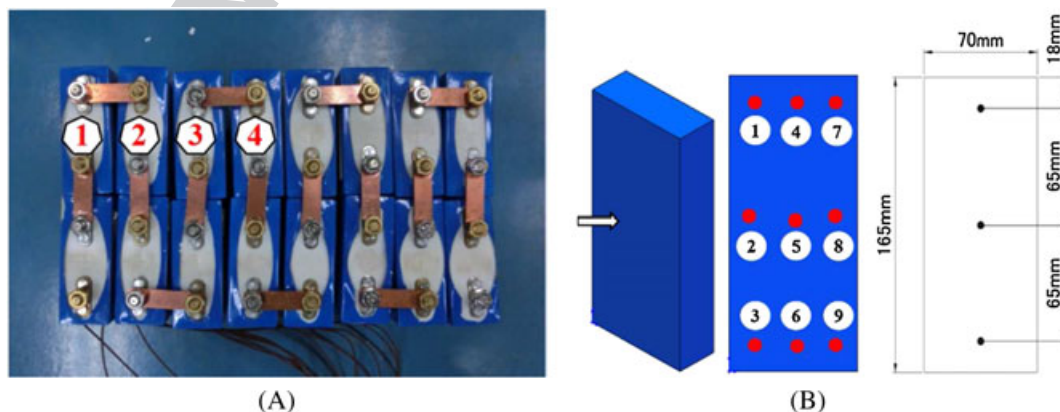
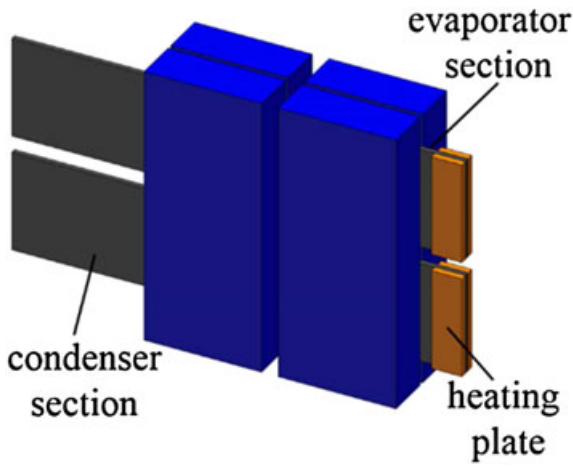


FIGURE 1 LiFePO<sub>4</sub> battery: (A) battery module; (B) thermocouples location [Colour figure can be viewed at wileyonlinelibrary.com]

F3

Colour online, B&W in print



**FIGURE 3** TMS diagram of lithium-ion battery [Colour figure can be viewed at wileyonlinelibrary.com]

### 2.3.2 | Heating method

The heating plate was installed on the evaporation section of MHPA. MHPA was heated by using plate. Then, the battery was heated. The installation method is presented in Figure 3.

## 3 | COOLING EXPERIMENTAL ANALYSIS

### 3.1 | Calculation of the area of dissipation in the condensation section

The module was encased in a container. Charge and discharge were controlled by a Neware EVT 500V300A, which produced constant currents of 18 and 36 A to the cut-off voltage. The cut-off voltages for charge and discharge were 2.5 and 3.6 V,<sup>17</sup> respectively. Temperature changes were recorded using Agilent 34970A data acquisition. Heat generation was calculated in accordance with the theoretical calculations proposed by Bernardi et al<sup>18</sup>:

$$Q = I(U-V) - I \left( T \frac{\partial U}{\partial T} \right) \quad (1)$$

The first term on the right-hand side is ohmic loss.  $U$  and  $V$  are the open circuit and cell operating potentials, respectively. The second term is the entropy heat generation term. Considering that battery reaction progresses are in reverse, the charge and discharge reactions are the reverse of one another. Thus, the second term of this equation is negligible during 1 charge and discharge cycle. Heat is assumed to be generated uniformly throughout the cell. Room temperature range was measured as 25–21 27°C. The value of heat generation is shown in Table 1.

**TABLE 1** The heat generate calculation of battery module

|    | Average temperature rise $\Delta T$ (°C) | Heat generation (W) |
|----|--|---------------------|
| 1C | 16.2                                     | 21.7                |
| 2C | 25.4                                     | 67.8                |

The battery charge and discharge processes follow the law of energy conservation with the following formula:

$$Q = Q_e + Q_a \quad (2)$$

where  $Q = 67.8$  W is heat generation during the 2C process and  $Q_a$  is the heat absorbed by the battery itself, indicating the performance of the battery temperature in the rise and fall. The average temperature at the end was assumed to 40°C by cooling, because the best operation temperature of the battery module was 25°C–40°C,<sup>19</sup> and  $\Delta T = 40^\circ\text{C} - 26.86^\circ\text{C} = 13.14^\circ\text{C}$ ,  $Q_a = 35.0$  W, where  $Q_e$  is the heat exchange between the battery and the environment. In this experiment,  $Q_e$ , the convection heat between the module and the air by MHPA, was 32.8 W.

The amount of heat transfer through the outer blowing condensation of MHPA is calculated by Equation 3:

$$Q_e = hA(T_{MHPA} - T_{air}) \quad (3)$$

where  $T_{MHPA}$  is the average temperature of condenser section;  $T_{air}$  is the average temperature of air;  $h$  is the convective heat transfer coefficient with fan wind speed = 2 m·s<sup>-1</sup> by forcing convection  $Gr$ ,  $Nu$ , and  $Re$ , and then calculated as  $h = 16.1$  W·m<sup>-2</sup>·K<sup>-1</sup>;  $A$  is the total area of the required condensing section calculated as  $A = 0.155$  m<sup>2</sup>. The thermocouple was arranged in the middle of the cell with a width of 60-mm MHPA. Each piece of MHPA in the condensation section was calculated as approximately 90 mm. Wu et al<sup>20</sup> demonstrated that forced convection could control battery temperature to a certain extent, but the surface temperature difference between the cells was too large. Figure 4 illustrates how the fan blew from the top down only through MHPA to achieve a forced convection effect.

In the charge-discharge cycle, the hourly module temperature difference is derived as follows:

$$\Delta T = T_{max} - T_{min} \quad (4)$$

where  $T_{max}$  and  $T_{min}$  are the maximum and the minimum, respectively, of 54 temperature measuring points in the module. Assuming that the difference between the surface temperature and inner temperature is negligible, the dissipating heat effect of the MHPA cooling method was evaluated by temperature comparison.

F4  
100  
101  
102  
103  
104  
105  
106  
107  
108  
109  
110  
111  
112  
113  
114

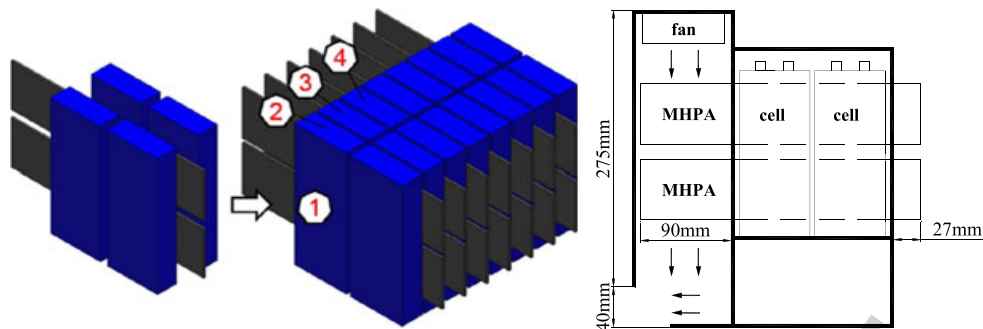


FIGURE 4 Schematic illustration of the models sealed in case [Colour figure can be viewed at wileyonlinelibrary.com]

### 3.2 | Comparison with traditional air-cooling method

The abovementioned air speed was used in forced convection, as illustrated in Figure 5A. The average temperature increases of the 8 cells at the 1C rate is depicted in Figure 5B. In Figure 5B, the heat dissipation of the front battery affected battery temperature, inevitably causing uneven temperature distribution within the module with the maximum temperature difference of 6°C. As the current increases, the temperature difference becomes more apparent. Given the high impact on battery life and performance, high magnification charge and discharge air cooling are inapplicable.

### 3.3 | Battery module 1C charge and discharge cycle test results

The traditional constant current 1C charge and discharge to cut-off voltage was conducted with 3-minute intervals for a total time of approximately 7200 seconds. The experiment was divided into 2 conditions, which were simultaneously conducted to ensure that environmental conditions remained constant. The average temperature curves of cells 1 to 4 are illustrated in Figure 6.

As shown in Figure 6, the temperature difference between the module and ambient air was minimal during

the charging process. Thus, the module temperature increased rapidly. The rate of temperature increase was approximately 8.5°C/hour. After the addition of MHPAs and the fan, the rate decreased to 5.7°C/hour. At the beginning of discharge, due to the interval time, the temperature gradient of the original module was gradual. Temperature increased rapidly in the middle of the discharge process. The internal battery resistance increased at the end of discharge, thus increasing the generated heat. Therefore, module temperature increased rapidly until the end of the discharge process. After the addition of MHPAs and the fan, temperature gradually decreased and reached 32°C, reflecting the heat-conducting property of MHPA.

Heat generation was different because the cell impedance was different. Furthermore, the cells in the middle of the module were influenced by the heat from the surrounding cells, causing differences in temperature. The hourly temperature differences are illustrated in Figure 7.

Based on symmetry, the temperature difference of the 4 cells was estimated as the temperature difference of the entire module. Figure 7 shows that the temperature difference between the 2 trends is similar at 2°C by the end of the charging process. The temperature difference of the original module increased rapidly during the discharging process and reached 6°C at the end. After added MHPAs

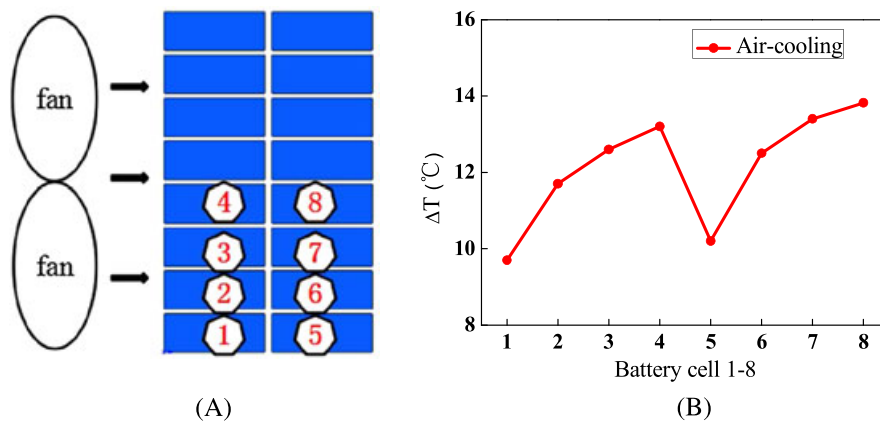
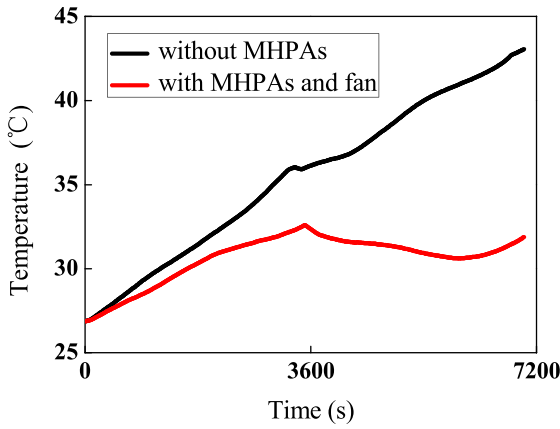


FIGURE 5 Air-cooling: (A) cooling method; (B) cell 1–8 temperature change [Colour figure can be viewed at wileyonlinelibrary.com]

Colour online, B&W in print

F7

Colour online, B&W in print



**FIGURE 6** Average temperature change curves of battery modules at 1C rate [Colour figure can be viewed at wileyonlinelibrary.com]

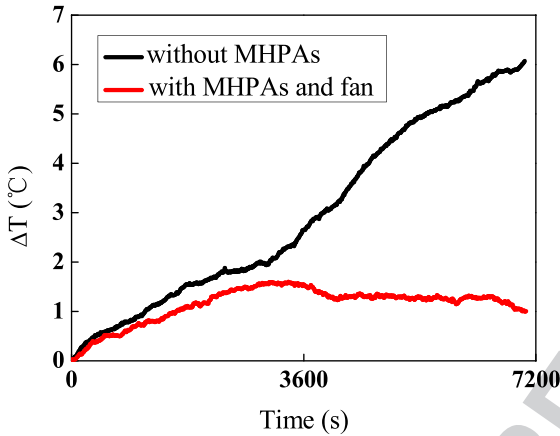


**FIGURE 7** Hourly temperature differences in the battery modules at 1C rate [Colour figure can be viewed at wileyonlinelibrary.com]

and the fan, the temperature difference gradually decreased to approximately 1.5°C at the end of the process. Pesaran<sup>21</sup> reported that the temperature difference between cells should be less than 5°C. Sabbah et al<sup>6</sup> found that battery temperature difference is great in an air-cooling system, especially when batteries are densely packed together, and the air-cooling effect is poor. In this experiment, the temperature difference of the battery module was maintained at 2°C, and the uniform thermal conductivity of MHPA was reflected.

### 3.4 | Battery module 2C charge and discharge cycle test results

The total time of the module charge and discharge to the cut-off voltage at a 2C rate was approximately 3600 seconds. The average temperature change curve of the module is depicted in Figure 8A. The chemical reaction was

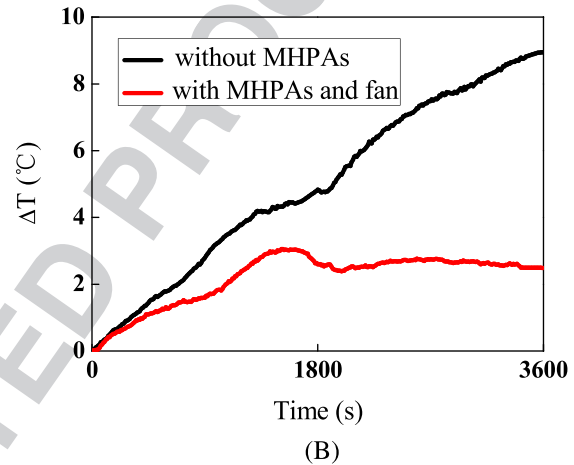
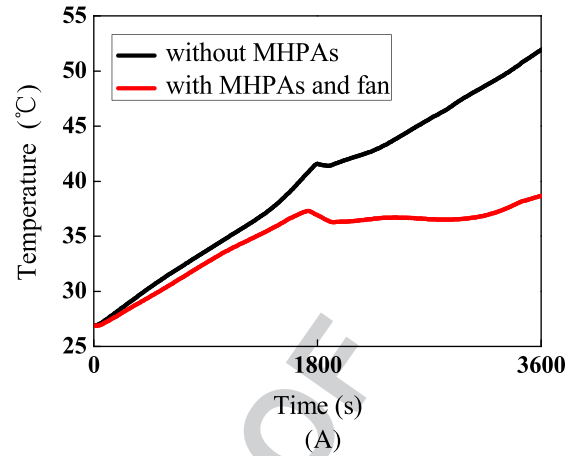


**FIGURE 8** Temperature change curves of battery modules at 2C rate: (A) average temperature; (B) hourly temperature differences [Colour figure can be viewed at wileyonlinelibrary.com]

active, and the irreversible heat was increased given that the module was in the 2C high rate charge and discharge. After the addition of the MHPAs and the fan, the temperature decreased by nearly 13°C and was 39°C at the end of the process, similar to the assumed temperature value of 40°C.

The temperature difference of the module is presented in Figure 8B. The temperature difference of the original module rapidly increased and reached 9°C at the end of the process. After the MHPAs and fan were added, the temperature difference curve was gradual and was less than 3°C at the end of the process.

## 4 | HEATING EXPERIMENTAL ANALYSIS

### 4.1 | Comparison with traditional heating method

In the traditional heating method, a heating film is used on the bottom of the directly heated battery. Thus, heat

Colour online, B&W in print

transfers from the bottom to the top of the battery. Room temperature was measured approximately 26°C, the battery was heated for 20 minutes (12 W), and at the same time using MHPA heating method with the same power, then temperatures were compared in Figure 9.

In Figure 9, the average temperature of the battery was increased to 14.5°C by heating MHPA. The temperature difference was less than 2°C. The average temperature of the traditional heating method increased by only 9°C. The temperature difference increased to 6°C. For the same heating time, the effect of MHPA heating was considerably better than the effect of the traditional method.

## 4.2 | Charge characteristics of the battery at low temperature

In practice, given that the lithium-ion batteries are not allowed to charge below 0°C because it would cause irreversible damage to the electrode material, it is required to heat the battery before charging (use of charging pile) in a cold environment, but battery is not afraid of discharge at low temperature. Cells were placed in a thermal chamber at a set temperature, allowed to stand for 10 hours, then charged at a constant current of 1/2 C with a cut-off voltage of 3.65 V and a charge curve at -30°C to 25°C, as illustrated in Figure 10. The values for the test are presented in Table 2.

As shown in Table 2, the charge capacity and voltage of the battery gradually decreased when the temperature decreased from 25°C to -30°C. Moreover, the battery was almost not charged when temperature decreased to -30°C and -20°C; the charge capacity in the constant current was one third of the battery rated capacity at -10°C.

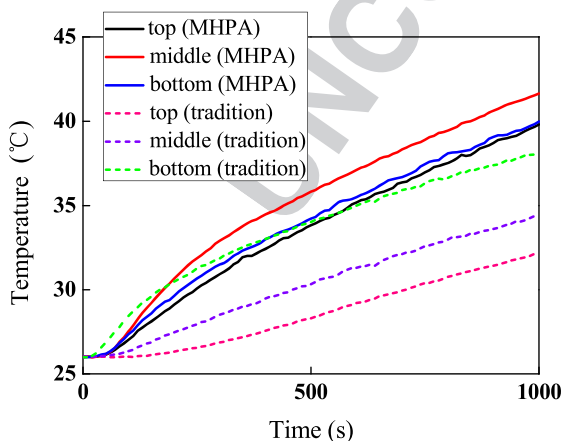


**FIGURE 9** Temperature curves of battery with traditional heating or heat pipe heating [Colour figure can be viewed at wileyonlinelibrary.com]

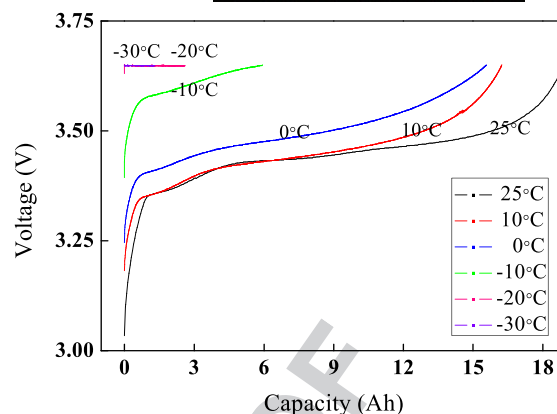


**FIGURE 10** Discharge curves of battery at different ambient temperatures [Colour figure can be viewed at wileyonlinelibrary.com]

**TABLE 2** Charge capacity and voltage at different temperatures

| Temperature (°C) | Charge capacity (Ah) | Charge voltage (V) |
|------------------|----------------------|--------------------|
| -30              | 1.31                 | 3.65               |
| -20              | 2.60                 | 3.63               |
| -10              | 5.93                 | 3.39               |
| 0                | 15.56                | 3.21               |
| 10               | 16.23                | 3.18               |
| 25               | 18.78                | 3.03               |

## 4.3 | Charge characteristics of the battery after MHPA heating

It is required to install the heating plates (30 W) with which the dimensions of the plate were 60 mm × 20 mm on the evaporation section of the above MHPAs. The battery was heated in a thermal chamber. It needs stopping heating up when the surface temperature of the battery reached 0°C. The battery was then charged at 9 A. The charge curve after heating is shown in Figure 11.

From top to bottom in the figure, the cures are as follows: the battery was heated from -30°C to 0°C, -20°C to 0°C, and -10°C to 0°C. The average charge voltage and capacity of the battery significantly increased after heating. The final charge capacity of the battery at -10°C and -20°C was slightly less than that at 0°C. When the battery was at -30°C, its charge capacity was slightly greater than that at 0°C because the residual heat of MHPA enabled the temperature to continuously increase to beyond 0°C while heat was exchanged between the battery and the low-temperature environment. The combination of both results indicated that small differences in

Colour online, B&W in print

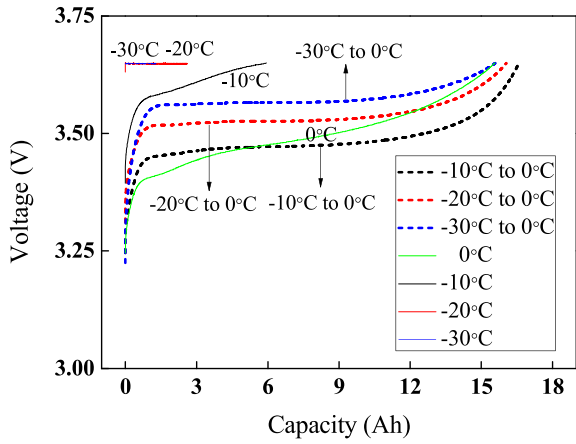


**FIGURE 11** Discharge curves of battery with/without heating [Colour figure can be viewed at wileyonlinelibrary.com]

**TABLE 3** Charge capacity and voltage at different temperatures after heating

| T (°C) | Charge capacity (Ah) |               | Charge voltage (V) |               |
|--------|----------------------|---------------|--------------------|---------------|
|        | Before heating       | After heating | Before heating     | After heating |
| -30    | 1.31                 | 15.59         | 3.65               | 3.22          |
| -20    | 2.60                 | 16.05         | 3.63               | 3.21          |
| -10    | 5.93                 | 16.58         | 3.39               | 3.20          |

battery temperature caused slight variations in charge capacity. The values for this test are displayed in Table 3.

As shown in Table 3, the charge capacity of the batteries was approximately 16 Ah after being heated in a low-temperature environment. The charge capacity increased 14.28 Ah at  $-30^{\circ}\text{C}$ , 13.45 Ah at  $-20^{\circ}\text{C}$ , and 10.65 Ah at  $-10^{\circ}\text{C}$ . Charge voltages increased to approximately 3.2 V.

Colour online, B&W in print

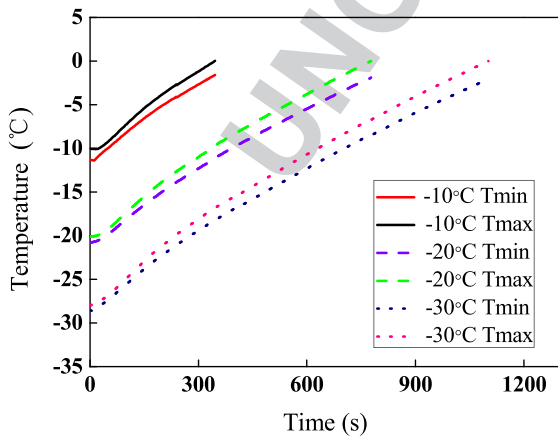


**FIGURE 12** Temperature curves of battery along with time [Colour figure can be viewed at wileyonlinelibrary.com]

#### 4.4 | Changes in battery temperature after heating

The measuring point was the same as the location of the cooling test. Figure 12 presents the lowest and the highest temperatures of the battery in different low-temperature environments. The heat transfer rate of the MHPA was fast with excellent uniformity. Temperature difference was less than  $2^{\circ}\text{C}$ , and the time required for heating from  $-10^{\circ}\text{C}$ ,  $-20^{\circ}\text{C}$ , and  $-30^{\circ}\text{C}$  to  $0^{\circ}\text{C}$  was approximately 350, 780, and 1100 seconds, respectively.

#### 5 | CONCLUSION

The new MHPA-based TMS of the battery module, according to the effective thermal conductivity and transmission characteristics of MHPA, could change the cooling and heating mode of condensation and evaporation. Besides, the installation of MHPAs was compact and flexible. This system realizes the ideal efficiency of a battery on charge and discharge cycles, decreases battery attenuation at high and low temperatures and effectively alleviates local thermal runaway, substantially increasing the safety performance of the battery module and improving charging performance.

1. The heat generated by the module was calculated with the assumption that the average temperature of the battery module at the end of the 2C charge-discharge cycle was  $40^{\circ}\text{C}$ . The area of heat dissipation for the MHPA condensing section was then obtained.
2. The final temperature of the battery module was  $32^{\circ}\text{C}$  and  $39^{\circ}\text{C}$  when subjected to charge-discharge at the 1C and 2C rate under sealed condition, respectively. At the end of the 2C cycle, the temperature was the same as the assumed temperature of  $40^{\circ}\text{C}$ , and the module temperature differences were controlled within  $3^{\circ}\text{C}$ .
3. After using MHPA heating method to improve battery performance at low temperature, charge capacity reached approximately 16 Ah after heating. At  $-30^{\circ}\text{C}$ , the charge capacity increased 14.28 Ah after heating for 1100 seconds, the charge voltage increased to 3.2 V, and the battery temperature difference was less than  $2^{\circ}\text{C}$ .

#### ORCID

Xin Ye <http://orcid.org/0000-0003-0239-8430>

## REFERENCES

1. Huang KD, Tzeng SC, Chang WC. Energy-saving hybrid vehicle using a pneumatic-power system. *Appl Energy*. 2005;81:1-18.
2. Somogye R. An aging model of Ni-MH batteries for use in hybrid-electric vehicles: the Ohio State University; 2004.
3. Williford RE, Viswanathan VV, Zhang JG. Effects of entropy changes in anodes and cathodes on the thermal behavior of lithium ion batteries. *J Power Sources*. 2009;189:101-107.
4. Alaoui C. Solid-state thermal management for lithium-ion EV batteries. *IEEE Transactions on Vehicular Technology*. 2013;62:98-107.
5. Weinert JX, Burke AF, Wei X. Lead-acid and lithium-ion batteries for the Chinese electric bike market and implications on future technology advancement. *J Power Sources*. 2007;172:938-945.
6. Sabbah R, Kizilel R, Selman JR, Al-Hallaj S. Active (air-cooled) vs. passive (phase change material) thermal management of high power lithium-ion packs: limitation of temperature rise and uniformity of temperature distribution. *J Power Sources*. 2008;182:630-638.
7. Thanh-Ha T, Souad H, Bernard D, Sebastien F. Experimental investigation on the feasibility of heat pipe cooling for HEV/ EV lithium-ion battery. *Appl Therm Eng*. 2014;63:551-558.
8. Ji Y, Wang CY. Heating strategies for Li-ion batteries operated from subzero temperatures. *Electrochim Acta*. 2013;107:664-674.
9. Nelson P, Dees D, Amine K, Henriksen G. Modeling thermal management of lithium-ion PNGV batteries. *J Power Sources*. 2002;110:349-356.
10. Khateeb SA, Farid MM, Selman JR, Al-Hallaj S. Design and simulation of a lithium-ion battery with a phase change material thermal management system for an electric scooter. *J Power Sources*. 2004;128:292-307.
11. Rao ZH. Research on heat transfer enhancement of lithium-ion power battery: Guangdong University of Technology; 2010.
12. Swanepoel G. Thermal management of hybrid electrical vehicles using heat pipes: Stellenbosch University; 2001.
13. Zhao YH, Zhang KR, Diao YH. Heat pipe with micro-pore tubes array and making method thereof and heat exchanging system. The United States, 2011.
14. Deng YC, Zhao YH, Wang W, Quan ZH, Wang LC, Yu D. Experimental investigation of performance for the novel flat plate solar collector with micro-channel heat pipe array (MHPA-FPC). *Appl Therm Eng*. 2013;54:440-449.
15. Wang YY, Diao YH, Zhao YH, Wang LC. Cooling property of flat micro-heat pipe arrays for lithium battery. *Chinese Journal of Power Sources*. 2014;38:1433-1436.
16. Wang HY, Deng YC, Hao LM, Zhao YH. Applied investigation on LED heat cooling equipment using flat micro-heat pipe arrays. *Semiconductor Technology*. 2012;37:240-244.
17. Liu DS, Chen BL. Study on performances of lithium iron phosphate battery. *Journal of Henan Institute of Science and Technology*. 2012;40:65-68.
18. Bernardi D, Pawlikowski E, Newman J. A review of thermal performance. *J Electrochem Soc*. 1985;132:5-12.
19. Ling ZY, Chen JJ, Fang XM. Experimental and numerical investigation of the application of phase change materials in a simulative power batteries thermal management system. *Appl Energy*. 2014;121:104-113.
20. Wu MS, Liu KH, Wang YY, Wan CC. Heat dissipation design for lithium-ion batteries. *J Power Sources*. 2002;109:160-166.
21. Pesaran AA. Battery thermal management in EVs and HEVs: issues and solutions. Advanced Automotive Battery Conference. Las Vegas Nevada, 2001.

**How to cite this article:** Ye X, Zhao Y, Quan Z. Thermal management system of lithium-ion battery module based on micro heat pipe array. *Int J Energy Res*. 2017. <https://doi.org/10.1002/er.3847>